Computational Study of the Reaction of $CH_2(X^3B_1)$ with CH_3OH

Jicun Li, Xinli Song, Zhe Peng, Hua Hou, and Baoshan Wang*

College of Chemistry and Molecular Sciences, Wuhan University, Wuhan 430072, People's Republic of China

Received: August 26, 2008; Revised Manuscript Received: September 18, 2008

The reaction of triplet methylene with methanol is a key process in alcohol combustion but surprisingly this reaction has never been studied. The reaction mechanism is investigated by using various high-level ab initio methods, including the complete basis set extrapolation (CBS-QB3 and CBS-APNO), the latest Gaussian-*n* composite method (G4), and the Weizmann-1 method (W1U). A total of five product channels and six transition states are found. The dominant mechanism is direct hydrogen abstraction, and the major product channel is $CH_3 + CH_3O$, involving a weak prereactive complex and a 7.4 kcal/mol barrier. The other hydrogen abstraction channel, $CH_3 + CH_2OH$, is less important even though it is more exothermic and involves a similar barrier height. The rate coefficients are predicted in the temperature range 200−3000 K. The tunneling effect and the hindered internal rotational freedoms play a key role in the reaction. Moreover, the reaction shows significant kinetic isotope effect.

I. Introduction

Methanol (CH_3OH) is a promising alternative fuel and additive. The reactions of CH_3OH with various radicals such as H, O, OH, HO_2, CH_3, F, Cl, and Br have been studied extensively. The reaction mechanisms have been revealed theoretically and the rate constants have been measured by using various experimental techniques.[1−7] The combustion model of methanol has also been build for practical use.[8] However, the reaction between CH_3OH and the methylene radical, $CH_2(X^3B_1)$, has not attracted any attention up to date. The only information for this reaction is available in a review article by Tsang in 1987,[9] in which the $CH_2 + CH_3OH$ reaction was assumed to be analogous to the $CH_3 + CH_3OH$ reaction.

The triplet methylene radical is one of the most important radicals in combustion. It can be formed in many methanol-forming processes, for example, the $CH_3 + OH$ reaction, via the collisional deactivation of the excited singlet CH_2 product. Therefore, the reaction of $CH_2(X^3B_1)$ with CH_3OH might play an important role in the combustion of methanol. To assess such an importance, this work presents a high-level ab initio quantum chemistry study of the title reaction. The reaction mechanism has been explored for various possible product channels and the temperature-dependent rate coefficients and the kinetic isotope effect have been calculated as well. This piece of theoretical work may simulate the experimental study of the title reaction.

II. Computational Methods

To obtain reliable structures and energies, four ab initio methods have been employed in the study, including the complete basis set extrapolation scheme (CBS-QB3 and CBS-APNO),[10] the Gaussian-*n* composite model (G4),[11] and the expensive Weizmann theory (W1U).[12] The geometries were optimized at the B3LYP/6-311G(d,p), QCISD/6-311G(d,p), B3LYP/6-31G(2df,p), and B3LYP/cc-pVTZ levels of theory, respectively. All the methods have been well calibrated in the calculations of the geometries and energies for the stable molecules, radicals, and the stationary points. Minima have all real frequencies. The transition state is characterized by its unique imaginary frequency. The energetic reaction path was calculated at the B3LYP/6-311G(d,p) level of theory by using the intrinsic reaction coordinate (IRC)[13] method to confirm that the transition state connects the designated reactants and products.

To check the reliability of the density functional theory in the geometrical optimization, two ab initio electron-correlation methods, namely, MP2/6-311G(d,p) and CCSD/cc-pVTZ, were used for this purpose besides the QCISD/6-311G(d,p) method in the CBS-APNO scheme. The W1U method was used to calculate the barrier heights for the key reaction paths on the basis of the CCSD/cc-pVTZ optimized geometrical parameters to compare with the original W1U data in order to check the geometrical dependence of the barrier heights.

All ab initio calculations were carried out with the Gaussian03 programs.[14] The subsequent kinetic parameters were calculated by using the statistical transition state theory as detailed below.

III. Results and Discussion

In this work a total of five reaction paths were investigated as follows:

$$CH_2(X^3B_1) + CH_3OH(X^1A') \rightarrow CH_3(X^2A_2'') + CH_3O(X^2A') \quad \Delta H^0 = -5.3 \pm 1.1 \text{ kcal/mol} \qquad \text{(R1)}$$

$$\rightarrow CH_3(X^2A_2'') + CH_2OH(X^2A) \quad \Delta H^0 = -14.7 \pm 0.8 \text{ kcal/mol} \qquad \text{(R2)}$$

$$\rightarrow CH_3CH^2(X_2A') + OH(X^2\Pi) \quad \Delta H^0 = -7.6 \pm 1.1 \text{ kcal/mol} \qquad \text{(R3)}$$

$$\rightarrow CH_2CH_2OH(X^2A) + H \quad \Delta H^0 = -1.8 \pm 2.5 \text{ kcal/mol} \qquad \text{(R4)}$$

* Corresponding author. E-mail: baoshan@whu.edu.cn. Fax: 8627-68754067.

10.1021/jp807598w CCC: $40.75
Published on Web 11/08/2008

$$\rightarrow CH_3OCH_2(X^2A) + H \quad \Delta H^0 = 5.7 \pm 2.5 \text{ kcal/mol} \tag{R5}$$

where the heats of reaction at 0 K were calculated by using the experimental enthalpies of formation of the reactants and the products.[15−18] The first three product channels are exothermic and the last two channels are somewhat endothermic. Channels R1 and R2 proceed via direct hydrogen abstraction mechanism. One of the hydrogen atoms of CH_3OH is abstracted by CH_2 to form the CH_3 radical. Evidently, the abstraction of the methyl-group hydrogen (channel R2) is more exothermic than the OH-group hydrogen abstraction (channel R1). Channels R3−R5 represent the S_N2-type displacement routes. It is noted that channel R2 can also take place via the displacement process. The optimized transition states are shown in Figure 1. The corresponding geometrical parameters are shown in Table 1. The calculated energetic data are listed in Table 2.

It is worth noting the difference of the calculated energies at different levels of theory. In view of the heats of reaction, all four ab initio methods give consistent data with a deviation of at most 1 kcal/mol. In comparison with the experimental data, the W1U method shows the best performance as expected. The error is only 0.1 kcal/mol except for channels R4 and R5 which have no definitive experimental value.s (For reference, the W1U calculated enthalpies of formation at 0 K for CH_2CH_2OH and CH_2OCH_3 radicals are −4.2 and 2.1 kcal/mol, respectively.) Regarding to the six transition states, the barrier heights calculated at the four levels of theory show significant fluctuation. This implies that the energy of the stationary point can be very sensitive to the employed ab initio level of theory. In the following discussion, the W1U data are used unless stated otherwise.

1. Reaction Mechanism. Channel R1 takes place via a direct hydrogen abstraction path (TS1). As can be seen from Figure 1 and Table 1, TS1 is an early barrier. The breaking OH bond is stretched by 0.18 Å. The forming H−C bond is about 0.27 Å longer than the equilibrium CH bond distance of the methyl radical. The reacting O---H---C geometry is nearly linear with about 5° of deviation. The bond angle of the methylene radical becomes much smaller. The barrier height is calculated to be 7.4 kcal/mol. The classical barrier height (i.e., without the ZPE correction) is 9.5 kcal/mol.

As could be seen from Table 1, the B3LYP optimized geometrical parameters for TS1 are very consistent, regardless of the basis sets 6-311G(d,p), 6-31G(2df,p), and cc-pVTZ employed. This indicates that the geometrical parameters are insensitive to the sizes of the basis sets. However, the explicit electron-correlation methods such as MP2, QCISD, and CCSD do give different optimized structures. Apparently, the MP2 geometries show the greatest difference from the B3LYP geometries, but the later appears to be closer to the higher level CCSD geometries. This is reasonable since the B3LYP wave functions always have minor spin contamination (less than 1% with respect to the expectation value of 2 for triplets) than MP2 and the single-reference CCSD theory includes more extensive correlation than MP2. Comparing the CCSD and the B3LYP geometrical parameters, the OH distance becomes slightly longer and the HC distance is shortened. In other words, the transition state tends to move forward to the product side. To check the influence of the geometrical parameters on the barrier height, the W1U theory was used to calculate the barrier height but with the CCSD/cc-pVTZ optimized TS1 geometry instead of the default B3LYP/cc-pVTZ geometry. The results are shown in Table 2. The barrier increases to 8.0 kcal/mol (10.1 kcal/mol without ZPE correction), which is about 0.6 kcal/mol higher than the value obtained with the original W1U level of theory. Therefore, the barrier height does not change significantly.

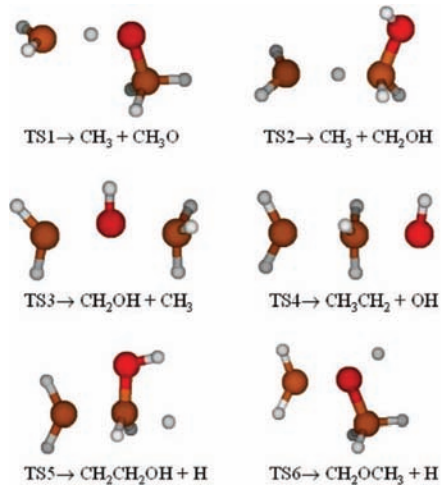

Figure 1. Structures of the transition states involved in the CH_2 + CH_3OH reaction. H: white ball. C: yellow ball. O: red ball.

Interestingly, the IRC calculation indicates that a prereactive complex exists along the abstraction pathway. The optimized geometry for this weakly bound complex is shown in the Supporting Information. The closest distance between the two fragments is O---HC, which is about 2.3 Å. The ZPE corrected binding energy is 0.8 kcal/mol and the classical binding energy is 1.9 kcal/mol. Evidently, this precursor is very weak. Such a shallow well cannot play a significant role in the reaction kinetics even at room temperature (e.g., the translational and rotational thermal energy at 300 K is $3RT \approx 1.8$ kcal/mol).

Channel R2 is the most exothermic route in the CH_2 + CH_3OH reaction. The reaction proceeds via TS2. One of the hydrogen atoms of the CH_3-group of CH_3OH is stretched by about 10%. The forming HC bond is still about 40% longer than the equilibrium length in the CH_3 radical. Evidently, TS2 is a reactant-like barrier. The reacting CHC geometrical angle is nearly linear. It is noted that TS1 shows C_s symmetry but TS2 is an unsymmetrical structure. The HCH plane of the CH_2 radical and the symmetrical plane HOCH of CH_3OH are distorted by about 100°. The barrier height is 6.9 kcal/mol, which is 0.5 kcal/mol lower than that of TS1. The classical barrier height is 8.1 kcal/mol, which is 1.4 kcal/mol lower than that of TS1. It is conceivable that the ZPE might play a more importance role in TS1. As shown in Table 2, TS1 has the smallest ZPE and thus the largest ZPE difference with respect to the reactants (e.g., $\Delta ZPE_{TS1} = -2.2$ kcal/mol).

As shown in Table 1, the B3LYP-optimized TS2 geometrical parameters with various basis sets show significant difference from the MP2, QICSD, and CCSD optimized geometries. Similar to TS1, the CCSD-optimized TS2 structure tends to be more product-like. The W1U energy was calculated by using the CCSD/cc-pVTZ optimized TS2 geometry and the results are shown in Table 2. The barrier height is 7.0 kcal/mol (8.2 kcal/mol without the ZPE correction), which is only 0.1 kcal/mol larger than the original W1U value in which the B3LYP/cc-pVTZ geometry is used. This checking confirms that the absolute barrier height is not sensitive to the geometrical parameters. The relative difference between TS1 and TS2 becomes 1.0 kcal/mol if the CCSD optimized geometries are used, in comparison with the value of 0.5 kcal/mol with the B3LYP optimized geometries. Considering the high barrier, such a difference is only marginal.

TABLE 1: Geometrical Parameters for the Transition States (TS1−TS6) Involved in the $CH_2 + CH_3OH$ Reaction[a]

species	coordinates	B3LYP/ 6-311G(d,p)	B3LYP/ 6-31G(2df,p)	B3LYP/ cc-pVTZ	MP2/ 6-311G(d,p)	QCISD/ 6-311G(d,p)	CCSD/ cc-pVTZ	CASSCF(8,7)/ 6-311G(d,p)
TS1	CH	1.354	1.356	1.348	1.223	1.286	1.283	1.304
	HO	1.132	1.128	1.139	1.223	1.176	1.179	1.210
	CHO	173.0	172.4	174.2	170.3	171.4	172.1	172.7
	HCH	127.6	127.3	127.6	124.6	125.8	126.1	124.4
	ϕ_{HCOC}	91.5	91.3	91.5	91.4	91.2	90.9	93.1
TS2	CH	1.505	1.511	1.494	1.397	1.414	1.414	1.407
	HC	1.231	1.228	1.234	1.262	1.272	1.267	1.337
	CHC	179.1	176.8	177.8	176.4	176.6	174.8	178.5
	HCH	124.8	124.6	124.7	123.4	123.5	123.8	122.5
	ϕ_{HCCO}	48.7	51.2	46.2	36.8	38.0	41.6	43.2
TS3	CO	1.790	1.779	1.789	1.696	1.782	1.770	1.854
	OC	1.780	1.770	1.781	1.726	1.798	1.789	1.903
	COC	161.0	162.2	162.0	160.1	164.9	165.8	169.6
TS4	CC	1.949	1.939	1.946	1.815	1.926	1.911	2.062
	CO	1.777	1.771	1.781	1.734	1.794	1.787	1.918
	CCO	178.2	178.6	178.6	177.5	178.9	179.3	178.6
TS5	CC	1.820	1.820	1.820	1.790	1.821	1.818	1.931
	CH	1.349	1.353	1.348	1.312	1.371	1.363	1.504
	CCH	168.8	169.0	168.7	168.9	168.2	168.6	164.9
TS6	CO	1.663	1.670	1.656	1.631	1.667	1.654	1.736
	OH	1.189	1.207	1.185	1.124	1.194	1.190	1.286
	COH	141.1	145.7	142.0	132.1	142.1	145.9	150.3

[a] Bond distances are in Å and angles are in deg.

TABLE 2: Energetic Data for the $CH_2 + CH_3OH$ Reaction Calculated at Various Levels of Theory[e]

species	ZPE	T_1[a]	c_{HF}[b]	QB3	APNO	G4	W1[c]	exptl[d]
$CH_2 + CH_3OH$	42.2			0	0	0	0	
RC	43.3	0.009	0.988	−0.7	−1.0	−1.3	−0.8	
TS1	40.0	0.012	0.977	5.7	5.9	6.8	7.4 (8.0)	
$CH_3 + CH_3O$	40.6			−5.9	−6.1	−6.3	−5.4	-5.3 ± 1.1
TS2	41.0	0.016	0.980	6.2	5.4	6.9	6.9 (7.0)	
$CH_3 + CH_2OH$	41.3			−14.5	−15.0	−14.9	−14.6	-14.7 ± 0.8
TS3	41.7	0.028	0.948	36.4	34.0	38.0	37.4	
TS4	42.4	0.032	0.944	35.4	34.1	38.0	37.3	
$C_2H_5 + OH$	41.7			−7.2	−7.9	−7.9	−7.5	-7.6 ± 1.1
TS5	41.0	0.013	0.960	45.5	44.7	47.6	46.6	
$C_2H_4OH + H$	39.7			0.9	1.0	0.8	1.0	-1.8 ± 2.5
TS6	40.1	0.026	0.963	44.1	43.0	44.1	44.2	
$CH_3OCH_2 + H$	40.4			6.1	6.2	6.6	7.3	5.7 ± 2.5

[a] T_1 diagnostic values calculated at the CCSD/cc-pVTZ level. [b] Coefficients of the dominant HF configuration calculated at the CASSCF(8,7)/6-311G(d,p) level. [c] The data in parentheses are calculated by using the CCSD/cc-pVTZ optimized geometries. [d] The experimental enthalpies of formations at 0 K are as follows (in kcal/mol): CH_3OH, -45.4 ± 0.1; CH_2, 93.4 ± 0.4; CH_3, 35.9 ± 0.1; CH_3O, 6.8 ± 0.5; CH_2OH, -2.6 ± 0.2; C_2H_5, 31.5 ± 0.5; OH, 8.9 ± 0.1; H, 51.6; C_2H_4OH, -5.5 ± 2.0; CH_2OCH_3, 2.0 ± 2.0 (see refs 15−18). [e] All the relative energies are calculated with respect to the $CH_2 + CH_3OH$ asymptote including the zero-point energies (ZPE) corrections. The B3LYP/cc-pVTZ ZPEs with a scaling factor of 0.985 are presented.

The remaining four transition states, namely TS3−TS6 for channels R2−R5, respectively, represent the S_N2-type displacement mechanism. Although most of these channels are energetically accessible, all channels involve significant barriers as high as 37−47 kcal/mol. Therefore, these reaction paths should not play any role in the $CH_2 + CH_3OH$ reaction. They are negligible and will not be discussed further.

The multiconfigurational characteristic is an important aspect for the open-shell species. In this work only the triplet potential energy surface was considered. At the reactant side, the singlet methylene lies ~9 kcal/mol above the triplet methylene.[15] For the transition states TS1 and TS2, the G4 calculated energies of the corresponding singlet states are 19.1 and 36.1 kcal/mol higher than those of the triplet states, respectively. This implies that the crossing between singlet and triplet potential energy surfaces is not significant for the present reaction. In fact, the reaction of singlet methylene with methanol takes place via a different mechanism from the triplet reaction.

To gain an insight on the significance of the multireference feature for the reaction of concern, two methods could be used. One is the T_1 diagnostic value of the coupled cluster wave function.[19] It has been shown that the multireference wave function is significant only if the T_1 diagnostic value is greater than 0.044.[20] As shown in Table 2, the T_1 diagnostic values calculated at the CCSD/cc-pVTZ level for all transition states are fairly small, i.e., 0.01−0.03. The other method is using the multireference SCF wave function. The stationary points of the $CH_2 + CH_3OH$ reaction are optimized by using the CASSCF(8,7)/6-311G(d,p) method.[21] The geometrical parameters are shown in Table 1 for comparison. The calculated geometrical parameters for TS1 and TS2 are in general agreement with the data obtained with either B3LYP or CCSD. The coefficients of the Hartree−Fock reference wave function are shown in Table 2. Evidently, all the coefficients are larger than 0.9, indicating that the single reference based ab initio methods used in this work should be applicable.

2. Reaction Kinetics. As discussed above, the major mechanism for the $CH_2(X^3B_1) + CH_3OH(X^1A')$ reaction includes two direct hydrogen abstraction pathways, namely,

$$CH_2 + CH_3OH \rightarrow RC \rightarrow TS1 \rightarrow CH_3 + CH_3O \quad (R1a)$$

$$CH_2 + CH_3OH \rightarrow TS2 \rightarrow CH_3 + CH_2OH \quad (R2a)$$

The reaction rate coefficients were calculated by using the conventional transition state theory with the rigid rotor harmonic oscillator approximations, viz.,

$$k(T) = \kappa \frac{Q^{\neq}}{Q_{CH_2} Q_{CH_3OH}} e^{-E_a/RT}$$

where κ is the tunneling factor and Q represents the total partition function including translation, rotation, vibration, and hindered internal rotation. E_a is the barrier height at 0 K. Since the two reaction paths both involve significant barriers, the variational effect should be negligible. The recrossing effect of the reaction flux has not been considered because it can be partially canceled by the variational effect. Therefore, the current treatment can give a good estimate to the upper-limit of the rate coefficients as a function of temperatures. The most important factors in such calculations include the treatment of the hindered internal rotors and the tunneling effect.

As indicated by the frequencies of TS1 and TS2, some vibrational modes should be considered as the hindered internal rotors. The automatic identification of the hindered internal rotors using the redundant internal coordinates is carried out using the methodology of Ayala and Schlegel.[22] All internal rotors are treated by using the multidimensional hindered rotational model and the corresponding partition function is calculated with use of Trular's formula,[23] viz.,

$$Q_i^{hin} = Q_i^{h.o.q} \tanh(Q_i^{free\ rot}/Q_i^{h.o.cl})$$

where $Q_i^{h.o.q}$ and $Q_i^{h.o.cl}$ are the quantum and classical partition function, the harmonic oscillator for the ith normal mode being treated as an internal rotation. $Q_i^{free\ rot}$ is the partition function calculated by using the free-rotor approximation, namely,

$$Q_i^{free\ rot} = \frac{(2\pi I_i kT)^{1/2}}{\hbar\sigma}$$

where k is Boltzmann's constant, $\hbar$ is Planck's constant divided by 2π, I_i is the effective moment of inertia, and σ is the effective symmetry number.

Two methods were employed to estimate the tunneling factor. One is the unsymmetrical Eckart potential model,[24] which is determined only by the imaginary frequency of the transition state, the barrier height, and the heat of reaction. The other is the semiclassical WKB approximation with the dual-level interpolation of the minimum-energy path (MEP).[25,26] The details of this methodology have been discussed elsewhere and we have used it successfully in the reaction of atomic oxygen with acetone.[27] Basically, the MEP was first calculated at a low level of theory such as B3LYP/6-311G(d,p), and then the individual energy along the MEP was extrapolated to the high level such as G4 or W1U. For TS1 and TS2, a total of 68 and 132 points along the MEP can be obtained at the B3LYP/6-311G(d,p) level of theory (see the Supporting Information). Note that the prereactive complex RC was considered explicitly in the calculation of the MEP of TS1. The calculated V_a^G data at various levels are shown in Figure 2. Evidently, the shapes of the MEP profiles for TS1 and TS2 are different. As a result, the tunneling effect for channels R1 and R2 should be considerably different.

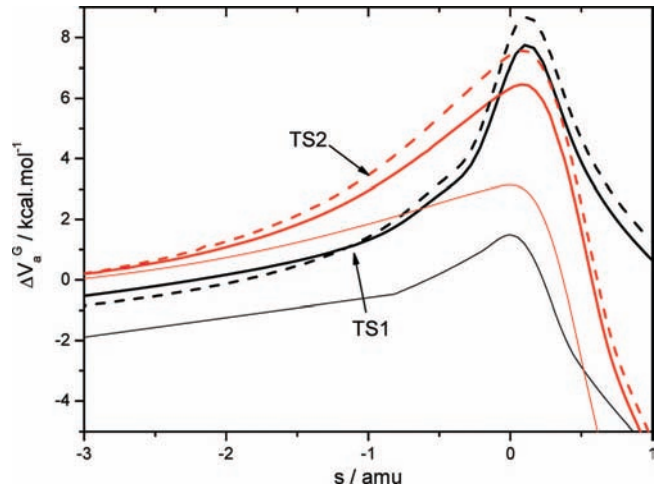

Figure 2. Minimum energy paths for the hydrogen abstraction reaction via TS1 (→ $CH_3 + CH_3O$, black lines) and TS2 (→ $CH_3 + CH_2OH$, red lines). Thin lines show the B3LYP/6-311G(d,p) calculated IRC energies along the reaction coordinates. Solid lines show the extrapolated V_a^G (MEP + ZPE) energies at the W1U level of theory. Dashed lines show the V_a^G energies for the isotopic reaction ($CD_2 + CD_3OD$).

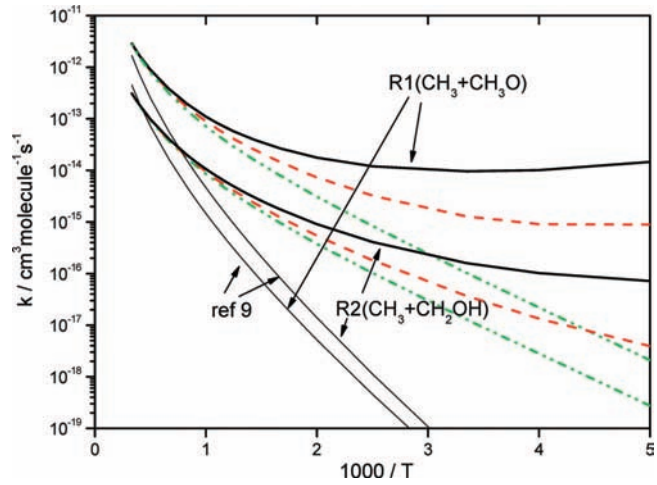

Figure 3. Arrhenius plots for the rate coefficients of the $CH_2 + CH_3OH$ reaction: thick solid lines—rate coefficients with the semiclassical WKB tunneling correction; dashed lines—rate coefficients with the Eckart tunneling correction; dot-dashed lines—rate coefficients without tunneling factor; thin solid lines—data in ref 9.

The rate coefficients were calculated as a function of temperature in the range 200−3000 K. The results are shown as the Arrhenius plots in Figure 3. It is evident that the rate coefficients for channel R1 are significantly higher than those for channel R2, although channel R1 involves a slightly higher barrier (7.4 vs 6.9 kcal/mol) and the degeneracy of the reaction path of channel R2 is three times larger than that of channel R1 (e.g., CH_3OH has three indistinguishable hydrogen atoms on the CH_3 group and only one hydrogen atom on the OH group). The reason for such a result is 2-fold. One is that the TS1 for channel R1 has a larger tunneling effect, as indicated by its more narrow MEP profile than that of TS2 (see Figure 2). The other is due to the hindered internal rotor. Both TS1 and TS2 involve three hindered internal rotors. However, the smallest internal rotational constant for TS1 is only 21 cm^{-1}, in comparison with the value of 104 cm^{-1} for TS2. Therefore, the internal rotational partition function for TS1 is much larger

TABLE 3: Input Parameters for the Transition State Theory Calculations of the Rate Coefficients for the H-Abstraction Reactions *R1* and *R2*

species	moment of inertia (I_a, I_b, I_c, amu·bohr^2)	harmonic vib freq and the reduced freq (cm^{-1}) and moment of inertia (amu·bohr^2) for internal rotors	vib freq (cm^{-1}) [a]
CH_2	1.04841, 7.13124, 8.17966		1056, 3122, 3361
CD_2	1.83213, 14.25153, 16.08366		791, 2231, 2522
CH_3OH	14.01965, 72.89167, 75.51298	300, 318, 0.24501	1046, 1083, 1171, 1375, 1482, 1496, 1511, 2985, 3027, 3102, 3830
CD_3OD	27.55810, 95.45130, 100.23022	218, 260, 0.4626	779, 903, 990, 1064, 1082, 1095, 1153, 2142, 2246, 2297, 2788
TS1	58.35305, 316.35741, 349.72528	(18, 23, 2.9256); (142, 146, 0.3120); (359, 443, 0.0037)	*1524i*, 182, 421, 596, 1000, 1040, 1070, 1171, 1236, 1282, 1448, 1457, 1511, 2982, 3037, 3052, 3122, 3308
TS1-D	80.10175, 398.34251, 428.51228	(13, 17, 5.5438); (103, 106, 0.5288); (265, 324, 0.007)	*1108i*, 157, 332, 549, 725, 774, 907, 942, 963, 1011, 1053, 1077, 1141, 2134, 2241, 2254, 2261,2474
TS2	61.24558, 374.25420, 411.73615	(59, 62, 0.5809); (248, 289, 0.0019); (388, 374, 0.0017)	*995i*, 121, 484, 542, 643, 1072, 1112, 1176, 1264, 1345, 1376, 1440, 1486, 3013, 3095, 3125, 3275, 3820
TS2-D	90.91486, 443.36235, 487.01706	(43, 45, 1.1900); (180, 233, 0.0018)	*757i*, 104, 290, 377, 414, 556, 782, 891, 956, 977, 1022, 1032, 1071, 1168, 2187, 2223, 2320, 2448, 2781

[a] Unscaled frequencies calculated at the B3LYP/cc-pVTZ level of theory. *i* represents imaginary frequency.

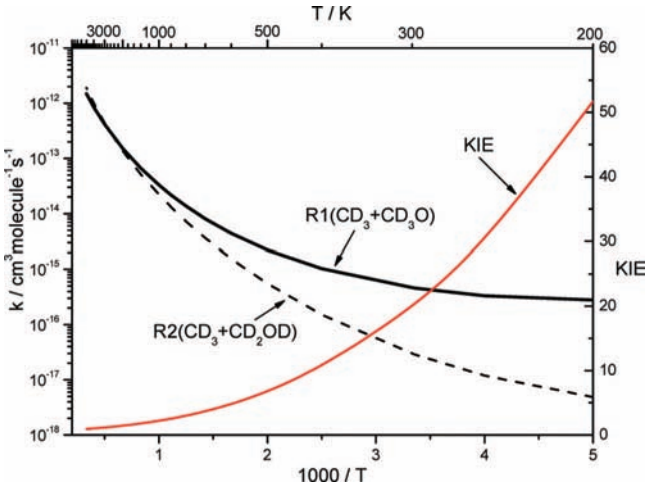

Figure 4. Arrhenius plots for the rate coefficients of the $CD_2 + CD_3OD$ reaction. KIE is shown as the red solid line attached to the right column.

than that of TS2 because more rotational energy levels can be populated in the case of TS1. As a result, even at temperatures above 2000 K, the contribution of the R1 channel to the overall reaction still accounts for more than 90%. It is conceivable that the major products of the $CH_2 + CH_3OH$ reaction should be CH_3 and CH_3O. This is in distinct contrast to the other analogous CH_3OH abstraction reactions. For example, in the H, CH_3, and $OH + CH_3OH$ reactions, the formation of $CH_3 + CH_2OH$ was shown to be the dominant channel with yields of more than 80% whereas CH_3O is only a minor product.[1,2]

As can be seen in Figure 3, the rate coefficient for channel R1 shows a slightly negative temperature dependence below 300 K. For example, the rate coefficient at 200 K is about 1.5 times larger than that at 300 K. This result is just caused by the extremely large tunneling effect for TS1 at lower temperatures. However, the simple Eckart tunneling effect model does not lead to the negative temperature dependence of the rate coefficients even down to 200 K, although the curve in Figure 3 shows typical non-Arrhenius behavior.

The abnormal temperature dependence of the rate coefficients at low temperatures could be an artifact since neither Eckart nor WKB determination of the tunneling factor would be conclusive. A new experimental study is desired to clarify this issue. Under the high-temperature combustion condition where the tunneling effect does not play a major role, for example, $T > 1000$ K, the rate coefficients mainly depend on the theoretical barrier heights. The inherent accuracy of the predicted barrier heights is hard to assess but presumably it can be 2 kcal/mol more or less in view of the data in Table 2. Therefore, the uncertainty of the predicted rate coefficients is a factor of 2 or even larger.

Previously, there is only one estimate of the rate coefficient of the title reaction.[9] In comparison with our theoretical data, as shown in Figure 3, the rate coefficients were underestimated considerably by a few orders of magnitude, especially at low to medium temperatures. Only at very high temperatures are the estimated data in agreement with our calculations. For practical use, the rate coefficients (in units of cm^3 molecule^{-1} s^{-1}) have been expressed by using the following two empirical formulas, viz.,

$$k_{R1}(T) = (4.20\times10^{-25})T^{3.52}\exp(1124/T) + (4.82\times10^{-22})T^{2.80}\exp(-618/T)$$

$$k_{R2}(T) = (1.01 \times 10^{-24})T^{3.11} \exp(300/T) + (6.61 \times 10^{-22})T^{2.52} \exp(-1116/T)$$

For completeness, the kinetic isotope effect (KIE) has been calculated for the $CD_2 + CD_3OD$ reaction. The vibrational frequencies and the internal rotors were calculated at the B3LYP/cc-pVTZ level of theory and the data are listed in Table 3. The rate coefficients and the KIE $= k_H/k_D$ are shown in Figure 4. In general, after the isotopic substitution, the rate coefficients become smaller. However, the rate coefficients for channel R2 become larger when temperatures increase above 600 K. As a result, both H-abstraction channels can play important roles to the overall reaction. At $T < 1000$ K, channel R1 is the dominant channel. At $T > 2000$ K, channel R2 becomes the major reaction channel. It is evident that the $CH_2 + CH_3OH$ reaction has a significant KIE. At 200 K, the KIE value is as high as 50. At room temperature, KIE = 20. These theoretical findings are worth being confirmed by new experimental measurements.

IV. Conclusions

The $CH_2(X^3B_1) + CH_3OH(X^1A')$ reaction has been studied theoretically for the first time. The energetic reaction routes were calculated by using the high-level ab initio methods including CBS-QB3, CBS-APNO, G4, and W1U. The reaction proceeds predominantly via two direct hydrogen abstraction paths, forming $CH_3 + CH_3O$ and $CH_3 + CH_2OH$, respectively. While the CH_2OH formation channel has a slightly lower barrier and is more exothermic, the rate coefficient calculation confirms that the CH_3O formation channel is dominant in the temperature range 200−3000 K. It is shown that the significant contributions from the internal rotational freedoms and the tunneling effect account for the CH_3O production via hydrogen abstraction. However, for the $CD_2 + CD_3OD$ reaction, the CD_2OD production might be competitive with the CD_3O channel, especially at elevated temperatures. Previous empirically estimated rate coefficients were seriously underestimated. New rate expressions for the title reaction are presented for practical use. The importance of the $CH_2 + CH_3OH$ reaction should be reconsidered in the current methanol combustion model. This theoretical work may simulate further experimental interests in methylene reactions.

Acknowledgment. This work is supported by the NSFC (No. 20603025 and 20673079), NCET-05-0618, and FANED (No. 200224).

Supporting Information Available: Table S1 lists the geometrical coordinates for all the species involved in the $CH_2 + CH_3OH$ reaction calculated at the B3LYP/cc-pVTZ level of theory, Table S2 lists the total energies of all the species at the CBS-QB3, CBS-APNO, G4, and W1U levels, Table S3 lists the energies of the MEP profiles for TS1 and TS2 calculated at the B3LYP/6-311G(d,p) level, and Figure S1 shows the prereactive complex for the H-abstraction channel R1. This material is available free of charge via the Internet at http://pubs.acs.org.

References and Notes

(1) Jodkowski, J. T.; Rayez, M-T.; Rayez, J-C.; Berces, T.; Dobe, S. *J. Phys. Chem. A* **1998**, *102*, 9219. 9230; **1999**, *103*, 3750.
(2) Srinivasan, N. K.; Su, M. C.; Michael, J. V. *J. Phys. Chem. A* **2007**, *111*, 3951.
(3) Lu, C. W.; Chou, S. L.; Lee, Y. P.; Xu, S. C.; Xu, Z. F.; Lin, M. C. *J. Chem. Phys.* **2005**, *122*, 244314.
(4) Christensen, L. E.; Okumura, M.; Hansen, J. C.; Sander, S. P. *J. Phys. Chem. A* **2006**, *110*, 6948.
(5) Anastasi, C.; Hancock, D. U. *J. Chem. Soc., Faraday Trans.* **1990**, *86*, 2553.
(6) Taketani, F.; Takahashi, K.; Matsumi, Y.; Wallington, T. J. *J. Phys. Chem. A* **2005**, *109*, 3935.
(7) Lendvay, G.; Berces, T.; Marta, F. *J. Phys. Chem. A* **1997**, *101*, 1588.
(8) Li, J.; Zhao, Z.; Kazakov, A.; Chaos, M.; Dryer, F. L., Jr *Chem. Kinet.* **2007**, *39*, 109.
(9) Tsang, W. *J. Phys. Chem. Ref. Data* **1987**, *16*, 471.
(10) Montgomery, J. A., Jr.; Ochterski, J. W.; Petersson, G. A. *J. Chem. Phys.* **1994**, *101*, 5900, and references cited therein.
(11) Curtiss, L. A.; Redfern, P. C.; Raghavachari, K. *J. Chem. Phys.* **2007**, *126*, 084108.
(12) Martin, J. L.; Oliveira, G. *J. Chem. Phys.* **1999**, *111*, 1843.
(13) Gonzalez, C.; Schlegel, H. B. *J. Phys. Chem.* **1990**, *94*, 5523.
(14) Frisch, M. J.; Trucks, G. W.; Schlegel, H. B.; et al. *Gaussian 03*, Revision D.01; Gaussian, Inc.: Pittsburgh, PA, 2003.
(15) Ruscic, B.; Boggs, J. E.; Burcat, A.; et al. *J. Phys. Chem. Ref. Data* **2005**, *34*, 573.
(16) Fleurat-Lessard, P.; Rayez, J. C.; Bergeat, A.; Loison, J.-C. *Chem. Phys.* **2002**, *279*, 87.
(17) Holmes, J. L.; Lossing, F. P. *Int. J. Mass. Spectrom, Ion Processes* **1984**, *58*, 113.
(18) Ruscic, B.; Berkowitz, J. *J. Chem. Phys.* **1994**, *101*, 10936.
(19) Lee, T. J.; Taylor, P. R. *J. Quant. Chem. Symp.* **1989**, *23*, 199.
(20) Rienstra-Kiracofe, J. C.; Allen, W. D.; Schaefer, H. F., III *J. Phys. Chem. A* **2000**, *104*, 9823.
(21) Frish, M. J.; Ragazos, I. N.; Robb, M. A.; Schlegel, H. B. *Chem. Phys. Lett.* **1992**, *189*, 524.
(22) Ayala, P. Y.; Schlegel, H. B. *J. Chem. Phys.* **1998**, *108*, 7560.
(23) Truhlar, D. G. *J. Comput. Chem.* **1991**, *12*, 266.
(24) Johnston, H. S.; Heicklen, J. *J. Phys. Chem.* **1962**, *66*, 532.
(25) Garrett, B. C.; Truhlar, D. G. *J. Phys. Chem.* **1979**, *83*, 2921.
(26) Hu, W.-P.; Liu, Y.-P.; Truhlar, D. G. *J. Chem. Soc., Faraday Trans.* **1994**, *90*, 1715.
(27) Hou, H.; Li, Y. Wang, B. *J. Phys. Chem. A* **2006**, *110*, 13163.

JP807598W